Viscoplastic Constitutive Modeling of Polymers—Flow Rules and the Plane Strain Response

J. Sweeney, S. Naz,* P. D. Coates

School of Engineering, Design and Technology/IRC in Polymer Science and Technology, University of Bradford, Bradford BD7 1DP, United Kingdom

Received 17 April 2008; accepted 19 June 2008
DOI 10.1002/app.29080
Published online 22 October 2008 in Wiley InterScience (www.interscience.wiley.com).

ABSTRACT: Plane strain compression tests, measuring both axial and transverse forces, are performed on ultra-high molecular weight polyethylene up to true axial strains of −0.4. As the deformation proceeds, the transverse stress becomes an increasing proportion of the axial stress, with the proportion growing from its initial value of 0.5 up to a value of 0.8. A constitutive model is applied that combines Ogden models and Eyring processes. It is found that when a Levy-Mises flow rule is used in conjunction with the Eyring model, the predicted ratio of transverse to axial stress remains much smaller than that observed, and is not greatly affected by changes in the Ogden exponent. However, when the flow rule is replaced by one that incorporates strain-induced anisotropy, realistic predictions are possible. For each Ogden model, we associate a flow rule for which the transverse strains in both the Ogden and Eyring models are individually zero. © 2008 Wiley Periodicals, Inc. J Appl Polym Sci 111: 1190–1198, 2009

Key words: Eyring process; hyperelasticity; flow rule

INTRODUCTION

As polymers become used increasingly in structural applications, there is a need for precise and quantitative understanding of their mechanical behavior. This is a nontrivial issue, since polymers become nonlinear at moderate strains and exhibit creep, stress relaxation, and strain-rate dependent yielding. Any constitutive model should reflect these considerations, while at the same time being useable in engineering analyses. Experimental investigations are required to define model parameters, and in many cases the models are too complex for the data from the customary uniaxial experiments to be sufficient for this purpose. This has been established for a large-strain elastic model of polypropylene by Sweeney et al.[1] who used plane strain extension of sheet specimens to finalize the model parameters. Other workers[2,3] have used plane strain compression for similar purposes. The state of plane strain is more general than the uniaxial state as all three principal strains are different from one another, and it can be a crucial source of information, particularly if both axial and transverse stresses are measured. In this article, we address the problem of an engineering polymer with exacting requirements, and show how plane strain data can have an important role in the development of the constitutive model.

For constitutive modeling, we have adopted the established technique of combining the Eyring process with hyperelastic network models. The Eyring process results in an appropriate form of the dependence of stress on time and rate of strain. To complete the specification of the plastic behavior, a flow rule is required, the form of which is a subject of discussion here. For a model to be successful, its predictions must include the correct relationship between the axial and transverse stresses in plane strain. We show that this condition is much easier to achieve when the hyperelastic model and the flow rule are related in a particular way. We describe a form of flow rule that includes strain-induced anisotropy, and establish corresponding sets of Ogden[4] hyperelastic models and flow rules of this form that possess the desired relationship.

Although our treatment involves anisotropy, the material is assumed to be initially isotropic. The anisotropy evolves with strain, purely as the result of the behavior of the hyperelastic model; the stiffnesses in the different principal directions are functions of the principal strains, and become significantly so at large deformations. This distinguishes our material models from those of initially anisotropic polymers, the most elementary being of oriented polymers such as fibers, where the small-strain elastic properties are of interest.[5] At large strains, there have been other elastic models of initially anisotropic materials, the most fundamental

**Present address:* Ford Motor Company, Dagenham Diesel Centre, Kent Avenue, Dagenham RM9 6SA, United Kingdom

Correspondence to: J. Sweeney (j.sweeney@bradford.ac.uk).

being defined by the "neoclassical" strain energy function, a generalization of the Gaussian model in which chains are initially anisotropic and characterized by a chain shape.[6] Other more recent approaches to orthotropic hyperelasticity are due to Bischoff et al.,[7] Horgan and Saccomandi,[8] Ehret and Itskov,[9] and Ogden and Saccomandi.[10] Thus, a number of instances of anisotropic hyperelasticity have been developed, mainly for rubbers and biological materials, that could be applied more generally to polymers if rate-dependent and yielding behavior could be combined with them to give a more realistic model. The question of how to introduce plasticity into these systems in a way that takes account of anisotropy has been addressed by a relatively few workers, notably Van Dommelen and Meijer,[11] working in the context of particle-modified polymers. They model strain-induced anisotropy via the effect of plastic strain on the yield strength in different material directions. Our approach outlined below, while showing some similarity, attacks the problem via the direct effects of strain upon the flow rule. We outline a method of adding plasticity into a hyperelastic model in such a way as to essentially preserve its three-dimensional response. Having established a hyperelastic model with a qualitative response (in terms of the ratios of principal stresses for a particular strain) appropriate for a given material, it then becomes possible to generalize to an elastic–viscoplastic model that still possesses the essentials of the desired behavior.

MATERIAL AND EXPERIMENTATION

In all tests ultra-high molecular weight polyethylene (UHMWPE) grade GUR1050 was used, manufactured by Hoechst and supplied by Orthoplastics, Lancs. UK in the form of blocks produced by large-scale compression molding using a proprietary process. This form of processing customarily results in isotropic material; evidence for the mechanical isotropy of the material used here is presented below at the end of this section. The molar mass of this grade of polymer has been estimated in the range 5.5–6.0 $\times 10^6$ g mol^{-1} using intrinsic viscosity measurements.[12] The crystallinity of the sample was determined at a value of 40.96% as quantified using Modulated Differential Scanning Calorimetry performed on a TA Instruments Q2000 DSC imposing a ± 0.5°C oscillation every 40 s onto a mean temperature ramp of 5°C min^{-1}. The area under the nonreversing heat capacity curve was divided by the heat of fusion for a 100% crystalline sample, taken as 293 J g^{-1}.

Plane strain compression tests were carried out at room temperature using an Instron testing machine in conjunction with the custom fabricated plane strain cell shown in Figure 1. This device enables both axial and transverse forces to be monitored; the Instron load cell monitors the axial force and the transverse force is measured by the load cell shown. The Instron load cell was used as supplied, of 50 kN capacity and sampling at 50 Hz. The transverse load was measured by a compressive cell of 900*N* capacity (model LFH-71 supplied by RDP Electronics, Wolverhampton, UK) sampling at 1.25 Hz. No smoothing or noise filtering has been applied to the results presented here. Specimens were in the form of cubes of side nominally 10 mm (mean 10.12 mm; standard deviation 0.053 mm), with faces machined to an average surface roughness of 5–6 μm. Room temperature tests were conducted at constant speeds, corresponding to increasing true strain rates. Specimens were strained to a final extension ratio of 0.67, corresponding to a true strain of -0.4. The outputs from the axial Instron load cell and the transverse load cell were synchronized using the clearly observable load drop as the crosshead stopped at the end of the experiment.

The specimens could not be observed during testing, but their deformed states could be examined after removal from the test cell. Observations and measurements with digital calipers then indicated that the specimens retained their rectangular shapes, with all surfaces plane, parallel surfaces remaining parallel, and thus no sign of "barreling" type deformation associated with friction at the main bearing surfaces. The possibility of friction effects has been explored further by uniaxial tests on circular

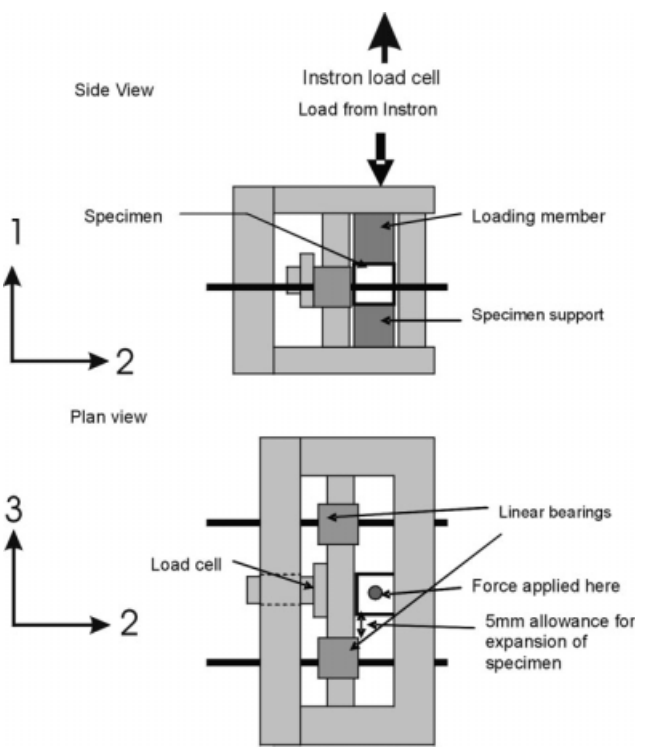

Figure 1 Plane strain cell.

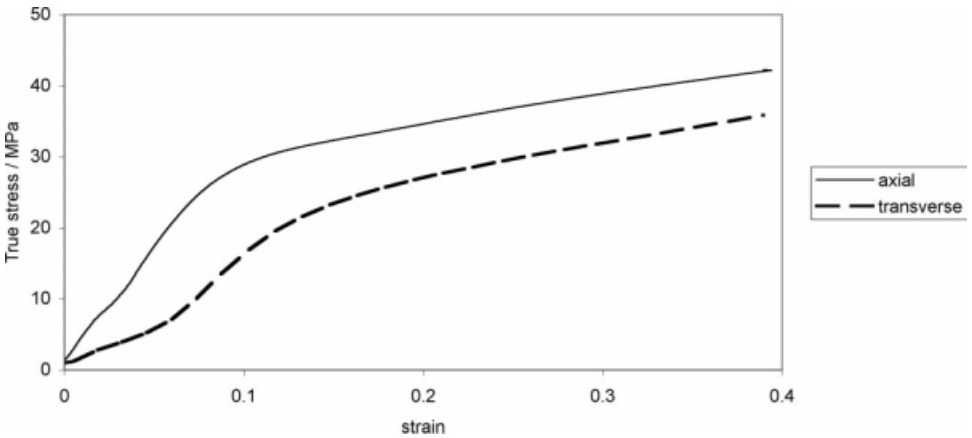

Figure 2 Stress–strain results (true stress and true strain) at initial strain rate of 0.0164 s^{-1}.

cylinders of the same material with bearing surfaces prepared in the same way. Cylinders of length 10 mm and height 10 mm were compressed between steel platens to true strains of −0.4 at strain rates in the range 5.0×10^{-4} to 1.9 s^{-1} using the Instron testing machine. Digital images of the specimen were captured immediately after unloading and the specimen diameters were measured as a function of axial distance. No changes in diameter were detectable except at the highest strain rate of 1.9 s^{-1}, in which case the central diameter exceeded the end diameters by 3%, giving a clearly barreled appearance. Thus, it was established that the deformation was uniform at strain rates up to 0.9 s^{-1}. The effects of friction were explored further using this test system by the use of petroleum jelly at the bearing surfaces. Operating at constant speed and at an initial strain rate of 0.0164 s^{-1}, the stress–strain curves for the two conditions—with and without lubricant—were found to be very close. At a true strain of −0.22, stresses were on average 30.75 MPa (three specimens; standard deviation 0.25 MPa) for unlubricated specimens and 30.73 MPa (six specimens, standard deviation 0.18 MPa) for lubricated specimens. We conclude that, at the strain rates used in the plane strain tests, frictional effects are negligible and the tendency for barreling is insignificant.

A typical stress–strain result is shown in Figure 2 for the initial strain rate of 0.0164 s^{-1}, where an average of five tests is presented. At the maximum compressive true strain of 0.4, the average axial stress and its standard deviation are 41.4 and 1.68 MPa, respectively. For the transverse stress, the corresponding figures are 36.1 and 1.36 MPa. The axial stress–strain curve resembles those reported for uniaxial compression by Kurtz et al.,[13] with a point of inflection at around a strain value of 0.1. Yield points in this region have also been reported for other polyethylenes[14,15] and has been attributed to c-shear deformation within the lamellae.[16]

To evaluate the assumption that the material is initially isotropic, we examine the present results in combination with a larger set of similar experiments carried out at strain rates in the range 4×10^{-3} to 0.53 s^{-1}. Specimens were compressed in directions chosen randomly with respect to the directions associated with the original compression molding operation. By examining the experimental ratio of the true stresses σ_1 and σ_2, it would be possible to detect anisotropy in the initial material by observation of the statistical distribution of the ratio σ_1/σ_2, which remains essentially constant with respect to strain rate. Significant anisotropy would manifest itself as two or more peaks in the distribution. For the set of 42 experiments, the distribution of values taken at a true strain of −0.36 (shown in Fig. 3) is symmetric with a single central peak. The average ratio is 1.21, with a prominent central peak of values in the range 1.19–1.23. We conclude that no significant mechanical anisotropy is detectable.

CONSTITUTIVE MODELING

General Theory

A basic element of the constitutive model is an elastic network in series with an Eyring process, such that the total deformation gradient $\mathbf{G}$ is split into elastic and plastic components $\mathbf{G}^e$ and $\mathbf{G}^p$, respectively:

$$\mathbf{G} = \mathbf{G}^e\mathbf{G}^p. \quad (1)$$

The basis of the numerical approach is to split the total deformation gradient into pure deformation $\mathbf{D}$ and rigid body rotation $\mathbf{R}$:

$$\mathbf{G} = \mathbf{DR}. \quad (2)$$

An incremental approach is used. During a given time step, the plastic stretch at the end of the previous time step is $\mathbf{D}_0^p$, $\Delta\mathbf{D}^p$ is the increment in plastic stretch during the current time step, and $\mathbf{D}^e$ is the

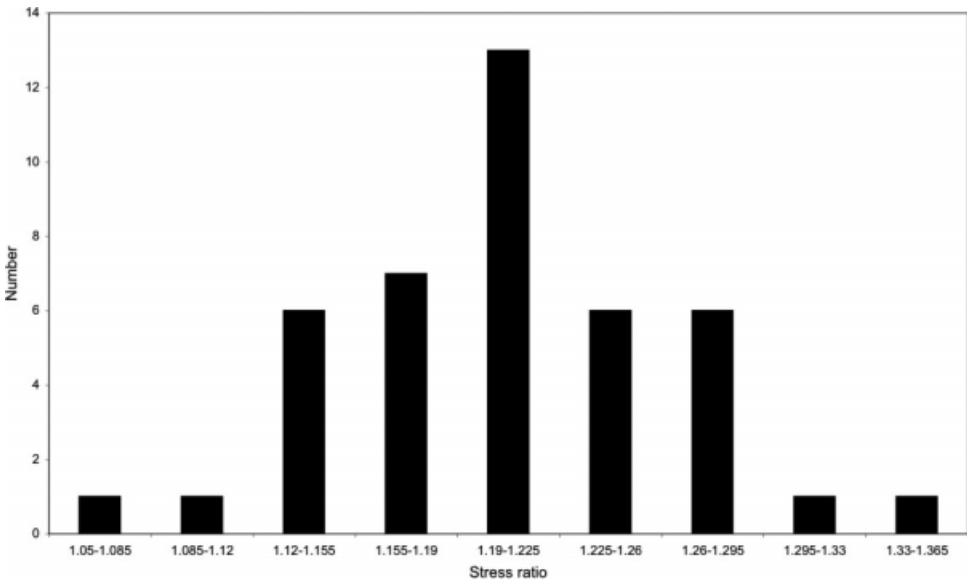

Figure 3 Distribution of values of the ratio axial stress/transverse stress for plane strain compression experiments taken at an axial true strain of −0.36.

elastic stretch. Then, the total deformation gradient **G** is

$$\mathbf{G} = \mathbf{D}^{\mathrm{e}}\Delta\mathbf{D}^{\mathrm{p}}\mathbf{D}_0^{\mathrm{p}}\mathbf{R}. \tag{3}$$

$\mathbf{D}^{\mathbf{e}}$, $\Delta\mathbf{D}^{\mathbf{p}}$, and $\mathbf{D}_0^{\mathbf{p}}$ include no rigid body rotations. $\mathbf{D}^{\mathbf{e}}$ and $\Delta\mathbf{D}^{\mathbf{p}}$ are collinear and share principal directions that are in general different from those of $\mathbf{D}_0^{\mathbf{p}}$. We follow the strategy of Bonet and Wood[17] and make the initial estimate of $\mathbf{D}^{\mathbf{e}}$ and $\mathbf{D}_{\mathrm{i}}^{\mathbf{e}}$, by assuming that there is no additional plastic strain:

$$\mathbf{D}_{\mathrm{i}}^{\mathrm{e}} = \mathbf{G}\mathbf{R}^{-1}\mathbf{D}_0^{\mathrm{p}-1}. \tag{4}$$

For a given total deformation **G**, $\mathbf{D}^{\mathbf{e}}$, and $\Delta\mathbf{D}^{\mathbf{p}}$ in eq. (3) are derived via an iterative process to impose the condition that the stresses in the network and the Eyring process are equal. Plane stress conditions are assumed. As justification for this, we note that, in our plane strain experiments, there is no stress applied to the specimen boundaries normal to the III direction, so that the only possible source of along this direction would be friction-induced shear at the other boundaries, which we have established in Section 2 to be negligible. $\mathbf{D}^{\mathbf{e}}$ defines the strain in the hyperelastic process and has principal components in the plane $\lambda_{\mathrm{I}}^{\mathrm{e}}$ and $\lambda_{\mathrm{II}}^{\mathrm{e}}$. Stresses may be defined in a variety of ways, one of which is by the one-term Ogden model:

$$\sigma_i = \mathbf{C}\left((\lambda_i^{\mathrm{e}})^n - (\lambda_{\mathrm{I}}^{\mathrm{e}}\lambda_{\mathrm{II}}^{\mathrm{e}})^{-n}\right) \quad i = \mathrm{I},\ \mathrm{II} \tag{5}$$

where σ_{I} and σ_{II} are principal stresses, C and n are material constants, and the assumption of incompressibility has been applied for the elastic strains.

In this "series" model, the stress in the hyperelastic network is the same as that in the Eyring process. For the latter, the scalar strain rate $\dot{\mathrm{e}}_{\mathrm{p}}$ is determined via the mean stress $\overline{\sigma}$ and a driving stress τ via the relation

$$\dot{\mathrm{e}}_p = A\,\exp(V_p\overline{\sigma})\sinh(V_s\tau) \tag{6}$$

where A, V_{p}, and V_{s} are material constants, the latter two being proportional to pressure and shear activation volumes, respectively, (following, e.g., Buckley and Jones[18] or Spathis and Kontou[19]). $\dot{\mathrm{e}}_{\mathrm{p}}$ is defined in terms of the tensor plastic strain rate $\mathbf{L}^{\mathbf{p}}$,

$$\dot{\mathrm{e}}_p = \sqrt{\frac{1}{3}\mathbf{L}^{\mathbf{p}} : \mathbf{L}^{\mathbf{p}}} \tag{7}$$

where the strain rate is itself defined in terms of the plastic deformation gradient as

$$\mathbf{L}^{\mathbf{p}} = \dot{\mathbf{D}}^{\mathbf{p}}\mathbf{D}^{\mathbf{p}-\mathbf{1}}. \tag{8}$$

To fully define $\mathbf{L}^{\mathbf{p}}$, we require the additional condition that it be collinear with the stress tensor, plus a flow rule. Rather than use a conventional Levy-Mises rule, we adopt a more general approach that allows for the development of anisotropy. Hill[20] produced a flow rule for orthotropic material. Adapting Hill's rule with $\mathbf{L}^{\mathbf{p}}$ defined along the directions of orthotropy with components $\mathrm{L}_{\mathrm{ij}}^{\mathrm{p}}$ and σ_{ij}, the components of the Cauchy stress in the same axes gives

$$\begin{aligned}
\mathrm{L}_{11}^{\mathrm{p}} &= \dot{\mathrm{e}}_p[H(\sigma_{11}-\sigma_{22}) + G(\sigma_{11}-\sigma_{33})]/3\tau \\
\mathrm{L}_{22}^{\mathrm{p}} &= \dot{\mathrm{e}}_p[F(\sigma_{22}-\sigma_{33}) + H(\sigma_{22}-\sigma_{11})]/3\tau \\
\mathrm{L}_{33}^{\mathrm{p}} &= \dot{\mathrm{e}}_p[G(\sigma_{33}-\sigma_{11}) + F(\sigma_{33}-\sigma_{22})]/3\tau \\
\mathrm{L}_{23}^{\mathrm{p}} &= \dot{\mathrm{e}}_p L\sigma_{23}/3\tau \\
\mathrm{L}_{13}^{\mathrm{p}} &= \dot{\mathrm{e}}_p M\sigma_{13}/3\tau \\
\mathrm{L}_{12}^{\mathrm{p}} &= \dot{\mathrm{e}}_p N\sigma_{12}/3\tau
\end{aligned} \tag{9}$$

where F, G, H, L, M, and N are anisotropy parameters. Equation (9) represents incompressible plastic flow. From the definition (7) of $\dot{e}_p$, it follows that the driving stress τ is given by

$$\tau = \sqrt{\frac{1}{3}\begin{pmatrix} [H(\sigma_{11}-\sigma_{22})+G(\sigma_{11}-\sigma_{33})]^2+[F(\sigma_{22}-\sigma_{33})+H(\sigma_{22}-\sigma_{11})]^2 \\ +[G(\sigma_{33}-\sigma_{11})+F(\sigma_{33}-\sigma_{22})]^2+2[L^2\sigma_{23}^2+M^2\sigma_{13}^2+N^2\sigma_{12}^2] \end{pmatrix}} \quad (10)$$

when $F = G = H = L = M = N = 1$, the relations (7) and (9) are equivalent to the Levy-Mises flow rule. When the anisotropy is strain-induced, the anisotropy parameters are initially unity. The principal planes of orthotropy are then determined by the strains in a manner that is particular to the material; it could be assumed that the principal total strain, principal elastic strain, or principal plastic strain would be the defining factor. Hill's flow rule has been mainly applied to metals, but there is no underlying physics that restricts it to any particular material type. It is a suitable model for strain-induced anisotropy, as the assumption of orthotropy enables us to make a direct association with principal directions of strain. There are precedents for its application to polymer systems.[11,21]

Plane Strain Application

For the experiments that concern us here as described above conducted using the apparatus of Figure 1, the three strains—total, elastic, and plastic—remain collinear and the directions of orthotropy are well defined. The form of experiment also ensures that the principal stresses remain collinear with the principal strains. In this simplified case, we may express the anisotropy parameters as a function f of principal strain. Then, the flow rule reduces to

$$\begin{aligned} \mathbf{L}_{\mathbf{I}}^{\mathbf{p}} &= \dot{\mathbf{e}}_{\mathbf{p}}[\mathbf{f}(\mu_{\mathbf{III}})(\sigma_{\mathbf{I}}-\sigma_{\mathbf{II}})+\mathbf{f}(\mu_{\mathbf{II}})(\sigma_{\mathbf{I}}-\sigma_{\mathbf{III}})]/3\tau \\ \mathbf{L}_{\mathbf{II}}^{\mathbf{p}} &= \dot{\mathbf{e}}_{\mathbf{p}}[\mathbf{f}(\mu_{\mathbf{I}})(\sigma_{\mathbf{II}}-\sigma_{\mathbf{III}})+\mathbf{f}(\mu_{\mathbf{III}})(\sigma_{\mathbf{II}}-\sigma_{\mathbf{I}})]/3\tau \\ \mathbf{L}_{\mathbf{III}}^{\mathbf{p}} &= \dot{\mathbf{e}}_{\mathbf{p}}[\mathbf{f}(\mu_{\mathbf{II}})(\sigma_{\mathbf{III}}-\sigma_{\mathbf{I}})+\mathbf{f}(\mu_{\mathbf{I}})(\sigma_{\mathbf{III}}-\sigma_{\mathbf{II}})]/3\tau \end{aligned} \quad (11)$$

where the μ_i are yet to be specified. Credible possibilities for the μ_i include principal total extension ratios λ_i, principal elastic extension ratios λ_i^e or principal plastic extension ratios λ_i^p. The arguments of f are determined by symmetry and to ensure initial isotropy $f(1) = 1$. The driving stress now becomes

$$\tau = \sqrt{\frac{1}{3}\begin{pmatrix} [\boldsymbol{f}(\mu_{\mathbf{III}})(\sigma_{\mathbf{I}}-\sigma_{\mathbf{II}})+\boldsymbol{f}(\mu_{\mathbf{II}})(\sigma_{\mathbf{I}}-\sigma_{\mathbf{III}})]^2 \\ +[\boldsymbol{f}(\mu_{\mathbf{I}})(\sigma_{\mathbf{II}}-\sigma_{\mathbf{III}})+\boldsymbol{f}(\mu_{\mathbf{III}})(\sigma_{\mathbf{II}}-\sigma_{\mathbf{I}})]^2 \\ +[\boldsymbol{f}(\mu_{\mathbf{II}})(\sigma_{\mathbf{III}}-\sigma_{\mathbf{I}})+\boldsymbol{f}(\mu_{\mathbf{I}})(\sigma_{\mathbf{III}}-\sigma_{\mathbf{II}})]^2 \end{pmatrix}}. \quad (12)$$

We now apply a deformation corresponding to incompressible plane strain, with

$$\lambda_{\mathbf{I}} = \lambda, \lambda_{\mathbf{II}} = 1 \text{ and } \lambda_{\mathbf{III}} = 1/\lambda. \quad (13)$$

The three direction is unrestrained, with

$$\sigma_{\mathbf{III}} = 0. \quad (14)$$

According to eqs. (1) and (13),

$$\lambda_{\mathbf{II}}^e \lambda_{\mathbf{II}}^p = 1. \quad (15)$$

We wish to explore the conditions when

$$\lambda_{\mathbf{II}}^e = \lambda_{\mathbf{II}}^p = 1. \quad (16)$$

This is true only when the condition (16) results in equilibrium, with both eq. (5) and the pair of eqs. (11) and (12) predicting the same stress σ_{II}; equally, the ratio $\frac{\sigma_{\mathrm{I}}}{\sigma_{\mathrm{II}}}$ must be the same for both the Ogden and Eyring models. For the Ogden model, with $\lambda_{\mathrm{I}}^e = \lambda^{\mathrm{e}}$ and with eq. (16), eq. (5) gives

$$\frac{\sigma_{\mathbf{I}}}{\sigma_{\mathrm{II}}} = (\lambda^e)^n + 1. \quad (17)$$

For (16) to apply for the Eyring process, the second of eqs. (11) must yield zero plastic strain rate. With eq. (13), this implies

$$0 = \boldsymbol{f}(\mu_{\mathbf{I}})\sigma_{\mathbf{II}} + \mathbf{f}(\mu_{\mathbf{III}})(\sigma_{\mathbf{II}}-\sigma_{\mathbf{I}}). \quad (18)$$

We now propose for the power law function f

$$f(\mu_i) = \mu_i^m \quad (i = \mathrm{I}, \mathrm{II}, \mathrm{II}) \quad (19)$$

and make the associations $\mu_{\mathbf{I}} = \lambda_{\mathbf{I}}^e$ and $\mu_{\mathbf{III}} = \lambda_{\mathbf{III}}^e$. Then, with $\lambda_{\mathbf{I}}^e = \lambda^e$ and with incompressibility giving $\lambda_{\mathbf{III}}^e = 1/\lambda^e$, (18) becomes

$$(\lambda^e)^m\sigma_{\mathbf{II}} + (\lambda^e)^{-m}(\sigma_{\mathbf{II}}-\sigma_{\mathbf{I}}) = 0 \quad (20)$$

or alternatively

$$\frac{\sigma_{\mathbf{I}}}{\sigma_{\mathbf{II}}} = (\lambda^e)^{2m} + 1. \quad (21)$$

Inspection of eqs. (17) and (21) reveals that eq. (16) is satisfied when $2m = n$. This reveals a set of

natural pairings of single-term Ogden models and flow rules of this power law form. It should facilitate the construction of effective viscoplastic models. Suppose, for a particular material, we have identified an Ogden model with realistic predictions of the stress ratio σ_I/σ_{II}; then, by the use of an appropriate flow rule, it becomes possible to add a plastic mechanism such that the principal stress ratio of the resulting model is substantially unchanged. The use of a conventional Levy-Mises flow rule (i.e., $f = 1$ in (11); $m = 0$ in (19)) in this context can greatly change the stress ratio of the combined model from that of the original Ogden model, simply because the softer mechanism in a series model will tend to dominate the overall behavior. These effects will be demonstrated further below.

We note that, for the eight-chain model of Arruda and Boyce[22] the principal stress ratio in plane strain is identical with that for the Gaussian model ($n = 2$), so the flow rule required for eq. (16) to apply corresponds to $m = 1$.

In the above treatment, we have adapted Hill's flow rule by assigning strain dependence to the anisotropy parameters F, G, H, L, M, N (eq. (9)). This is in contrast to the approach of Van Dommelen and Meijer,[11] and of Tzika et al.[21] who adapted Hill's yield criterion,[20] and fixed the values of the anisotropy parameters using their dependence on yield stresses, which are in turn determined by their dependence on plastic strain. Our approach, with its more direct involvement of strain rate via the flow rule, is a natural accompaniment to our use of the Eyring model.

MODELING OF EXPERIMENTS

In Figure 2, for both axial and transverse curves, we can identify a yielding process at a strain of around 0.1, followed by a decreased slope. This suggests that a two-arm model is the minimum requirement. The development above is for a single arm. In a two-arm model, the total stress tensor is the sum of the stress tensors in each arm, and the strain in each arm is identical. We assign the subscripts X and Y to the quantities in the respective arms. The development of the two-arm model proceeds straightforwardly, with eq. (1) being replaced by

$$\mathbf{G} = \mathbf{G}_{\mathbf{X}}^{\mathbf{e}}\mathbf{G}_{\mathbf{X}}^{\mathbf{p}} = \mathbf{G}_{\mathbf{Y}}^{\mathbf{e}}\mathbf{G}_{\mathbf{Y}}^{\mathbf{p}}. \tag{22}$$

The stresses are given by Ogden models as

$$\begin{aligned} \sigma_{iX} &= C_X(\lambda_i^n - (\lambda_I\lambda_{II})^{-n}) \\ \sigma_{iY} &= C_Y(\lambda_i^n - (\lambda_I\lambda_{II})^{-n}) \end{aligned} \quad i = I, II \tag{23}$$

where the principal directions in the two arms are generally different from each another, but coincide and are denoted by I and II in the modeling of the experiments here. Note that the same Ogden exponent is used in each arm. Two Eyring processes are defined by

$$\begin{aligned} \dot{e}_{pX} &= A_X \exp(V_{pX}\overline{\sigma}_X)\sinh(V_{sX}\tau_X) \\ \dot{e}_{pY} &= A_Y \exp(V_{pY}\overline{\sigma}_Y)\sinh(V_{sY}\tau_Y) \end{aligned}. \tag{24}$$

With $\sigma_{III} = 0$, the driving stresses from (11), using the same power law for f in each arm, are

$$\begin{aligned} \tau_{\mathbf{X}} &= \sqrt{\frac{1}{3}\begin{pmatrix} [\mu_{\mathbf{IIIX}}^{\mathbf{m}}(\sigma_{\mathbf{IX}} - \sigma_{\mathbf{IIX}}) + \mu_{\mathbf{IIX}}^{\mathbf{m}}\sigma_{\mathbf{IX}}]^2 \\ + [\mu_{\mathbf{IX}}^{\mathbf{m}}\sigma_{\mathbf{IIX}} + \mu_{\mathbf{IIIX}}^{\mathbf{m}}(\sigma_{\mathbf{IIX}} - \sigma_{\mathbf{IX}})]^2 \\ + [\mu_{\mathbf{IIX}}^{\mathbf{m}}(-\sigma_{\mathbf{IX}}) + \mu_{\mathbf{IX}}^{\mathbf{m}}(-\sigma_{\mathbf{IIX}})]^2 \end{pmatrix}} \\ \tau_{\mathbf{Y}} &= \sqrt{\frac{1}{3}\begin{pmatrix} [\mu_{\mathbf{IIIY}}^{\mathbf{m}}(\sigma_{\mathbf{IY}} - \sigma_{\mathbf{IIY}}) + \mu_{\mathbf{IIY}}^{\mathbf{m}}\sigma_{\mathbf{IY}}]^2 \\ + [\mu_{\mathbf{IY}}^{\mathbf{m}}\sigma_{\mathbf{IIY}} + \mu_{\mathbf{IIIY}}^{\mathbf{m}}(\sigma_{\mathbf{IIY}} - \sigma_{\mathbf{IY}})]^2 \\ + [\mu_{\mathbf{IIIY}}^{\mathbf{m}}(-\sigma_{\mathbf{IY}}) + \mu_{\mathbf{IY}}^{\mathbf{m}}(-\sigma_{\mathbf{IIY}})]^2 \end{pmatrix}} \end{aligned}. \tag{25}$$

The flow rule becomes

$$\begin{aligned} \mathbf{L}_{\mathbf{IX}}^{\mathbf{p}} &= \dot{\mathbf{e}}_{p\mathbf{X}}[\mu_{\mathbf{IIIX}}^{\mathbf{m}}(\sigma_{\mathbf{I}} - \sigma_{\mathbf{II}}) + \mu_{\mathbf{IIX}}^{\mathbf{m}}\sigma_{\mathbf{I}}]/3\tau_{\mathbf{X}} \\ \mathbf{L}_{\mathbf{IIX}}^{\mathbf{p}} &= \dot{\mathbf{e}}_{p\mathbf{X}}[\mu_{\mathbf{IX}}^{\mathbf{m}}\sigma_{\mathbf{II}} + \mu_{\mathbf{IIIX}}^{\mathbf{m}}(\sigma_{\mathbf{II}} - \sigma_{\mathbf{I}})]/3\tau_{\mathbf{X}} \\ \mathbf{L}_{\mathbf{IIIX}}^{\mathbf{p}} &= \dot{\mathbf{e}}_{p\mathbf{X}}[\mu_{\mathbf{IIX}}^{\mathbf{m}}(-\sigma_{\mathbf{I}}) + \mu_{\mathbf{IX}}^{\mathbf{m}}(-\sigma_{\mathbf{II}})]/3\tau_{\mathbf{X}} \\ \mathbf{L}_{\mathbf{IY}}^{\mathbf{p}} &= \dot{\mathbf{e}}_{p\mathbf{Y}}[\mu_{\mathbf{IIIY}}^{\mathbf{m}}(\sigma_{\mathbf{I}} - \sigma_{\mathbf{II}}) + \mu_{\mathbf{IIY}}^{\mathbf{m}}\sigma_{\mathbf{I}}]/3\tau_{\mathbf{Y}} \\ \mathbf{L}_{\mathbf{IIX}}^{\mathbf{p}} &= \dot{\mathbf{e}}_{p\mathbf{Y}}[\mu_{\mathbf{IY}}^{\mathbf{m}}\sigma_{\mathbf{II}} + \mu_{\mathbf{IIIY}}^{\mathbf{m}}(\sigma_{\mathbf{II}} - \sigma_{\mathbf{I}})]/3\tau_{\mathbf{Y}} \\ \mathbf{L}_{\mathbf{IIIX}}^{\mathbf{p}} &= \dot{\mathbf{e}}_{p\mathbf{X}}[\mu_{\mathbf{IIY}}^{\mathbf{m}}(-\sigma_{\mathbf{I}}) + \mu_{\mathbf{IY}}^{\mathbf{m}}(-\sigma_{\mathbf{II}})]/3\tau_{\mathbf{Y}} \end{aligned}. \tag{26}$$

This scheme has been implemented numerically as a user-defined subroutine (UMAT) in the finite element package ABAQUS. The results discussed below result from runs of the package at uniform strain. The implementation bears some similarity to the two-process scheme described by Sweeney et al.,[23] which was applied to the early stages of polymer deformation and made use of the conventional Levy-Mises flow rule.

TABLE I
Eyring Process Properties

V_{sX} (MPa^{-1})	V_{pX} (MPa^{-1})	V_{sY} (MPa^{-1})	V_{pX} (MPa^{-1})	A_X (s^{-1})	A_Y (s^{-1})
1.6	0.096	1.8	0.11	1.0×10^{-6}	1.4×10^{-8}

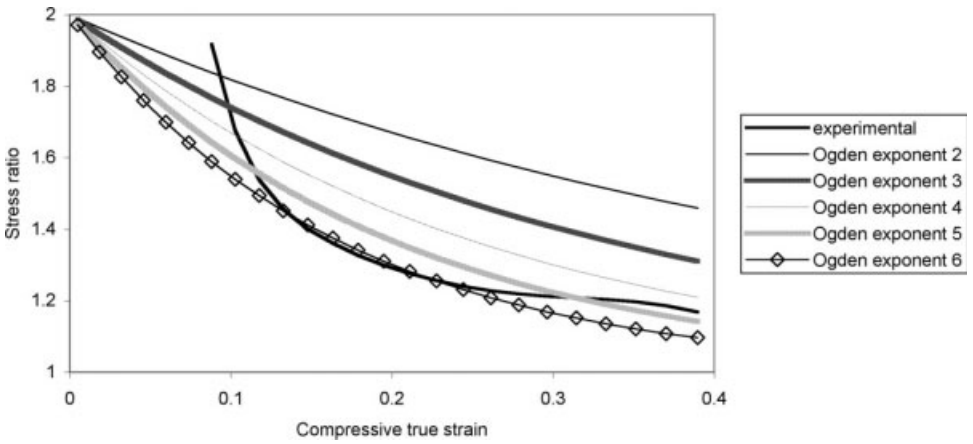

Figure 4 Experimental (rate 0.0164 s^{-1}) and Ogden stress ratios.

The required input data are the Ogden parameters C_X, C_Y and n; the Eyring parameters V_{pX}, V_{pY}, V_{sX}, V_{sY}, A_X and A_Y; and the flow rule exponent m. In the following analysis, we keep the Eyring parameters at fixed values, such as to be consistent with realistic levels of yield stress and its rate dependence, and explore the effects of varying the Ogden parameters and the flow rule. The Eyring parameters are listed in Table I. In line with the findings of other workers for glassy polymers such as Nazarenko et al.,[24] Bauwens-Crowet et al.,[25] and Govaert et al.,[26] we have assumed that $V_p = 0.06V_s$ to fix the values of V_{pX} and V_{pY}.

In Figure 4, we plot the experimental ratio σ_I/σ_{II} in plane strain compression (for initial strain rate 0.0164 s^{-1} corresponding to the results of Fig. 2) together with Ogden predictions of it for various exponent values. The intention here is to give guidance for the exponent value to be used in the model; it is a source of guidance only, as the total strain as measured experimentally differs from the elastic strain. The indication is that, of the possible choices, an n value in the range of 5–6 would be most appropriate.

We begin the modeling by establishing a baseline result using Gaussian networks ($n = 2$ in eq. (23)) and Levy-Mises flow rule ($m = 0$ in eqs. (25) and (26)). C_X and C_Y are assigned values 12 and 120 MPa, respectively, to give realistic predictions of σ_I. The results are plotted in Figure 5 in terms of the stress ratio σ_I/σ_{II} (case "$n = 2$, $m = 0$"). The ratio does not decrease greatly from the initial value of 2 and is in strong disagreement with the experimental result.

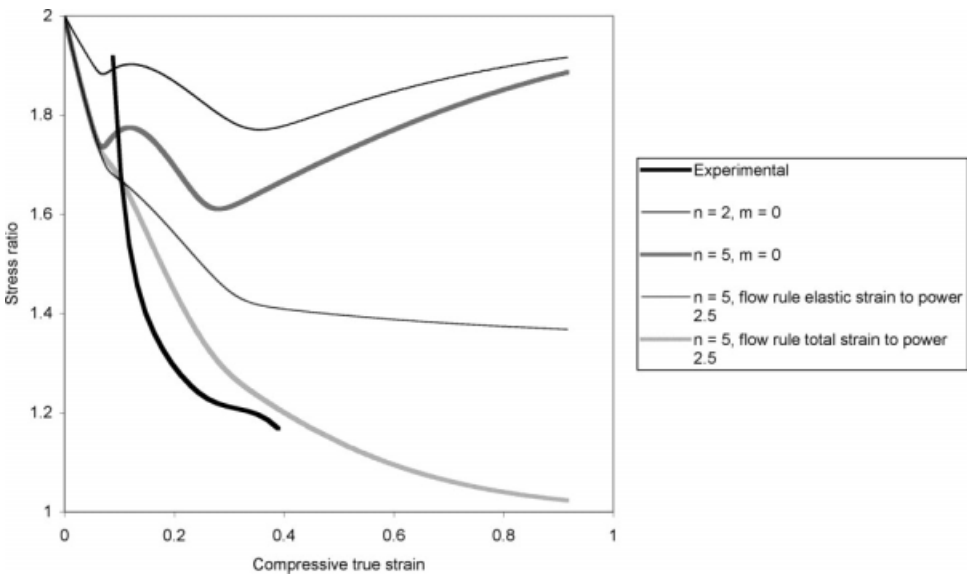

Figure 5 Experimental (rate 0.0164 s^{-1}) and model stress ratios for various Ogden model and flow rule combinations.

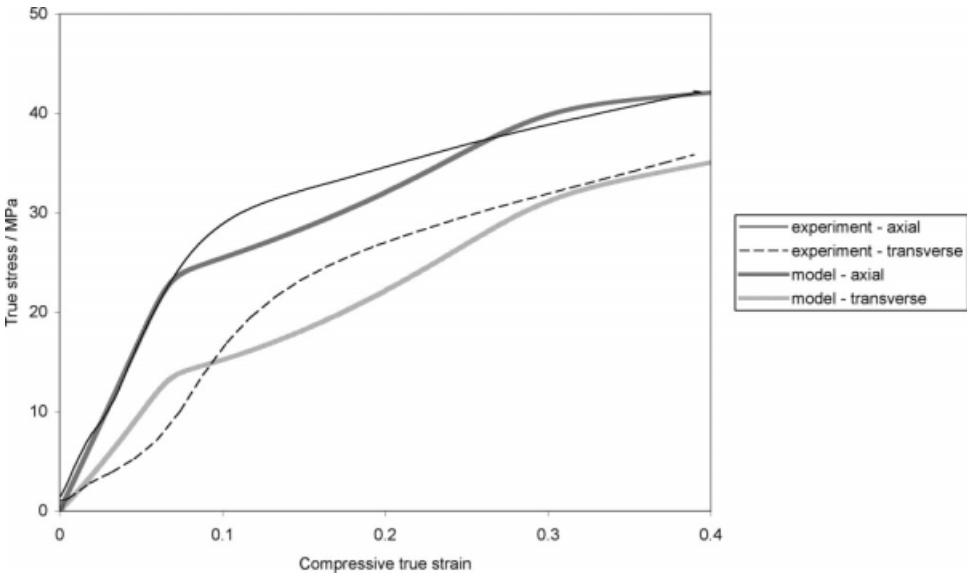

Figure 6 The case "$n = 5$, flow rule total strain to power 2.5" compared with the experimental result (rate 0.0164 s^{-1}).

We next use an Ogden model with a more realistic plane strain response, $n = 5$, but retain the Levy-Mises flow rule (case "$n = 5$, $m = 0$" in Fig. 5). The coefficients C_X and C_Y are assigned values 4.8 and 48 MPa, respectively, to produce elastic responses with the same initial slope as in the previous case where $n = 2$. The situation is slightly improved, but at larger strains the behavior is dominated by the flow rule and begins to resemble the $n = 2$ case.

For the third case, we use the same Ogden model with $n = 5$ together with a flow rule as given in eq. (26) with $m = 2.5$ and $\mu_i = \lambda_i^e$ (i = I, II, III). As argued above, since $m = 2n$ the response of the model in terms of σ_I/σ_{II} should resemble that of the Ogden model alone. As shown in Figure 5 (case "$n = 5$, flow rule elastic strain to power 2.5") the response is closer to that of the Ogden model, but the stress ratios are higher at any given strain compared with Figure 4. This is because the plot in Figure 5 is against total strain, whereas eqs. (17) and (21), and Figure 4, concern elastic strain.

In view of the above finding, we have examined the effectiveness of making the anisotropy in the flow rule a function of the total strain rather than the elastic strain. Thus, the flow rule is as given in (26) with $\mu_i = \lambda_i$ (i = I, II, III) and $m = 2.5$. The same Ogden model is again used with $n = 5$. The response is shown in Figure 5 as the case $n = 5$, flow rule total strain to power 2.5. Although it is by no means a good fit to the experiments, it is greatly more realistic than the predictions that use a conventional flow rule.

For this final case, the stress predictions are compared with the experiment in Figure 6. The relative simplicity of the model, with two processes only, results in yielding predictions that are more abrupt than is observed. However, the results are at a useful level. The model predictions for this form of verification are greatly improved in comparison with the other schemes considered.

CONCLUSIONS

Nonuniaxial experimental data are essential in the evaluation of constitutive models. Plane strain compression experiments on UHMWPE have shown that the transverse stress is greatly at variance with the predictions of a constitutive model that makes use of a conventional Levy-Mises flow rule. A Hill-type flow rule for anisotropic material, in which the anisotropy is strain-induced and governed by a power law function of extension ratio, has been shown to give much improved predictions when combined with an appropriate hyperelastic network model. A one-to-one correspondence between Ogden models and these flow rules has been established. When a corresponding pair is used within a series model of elastic and plastic elements, the transverse strain is zero in both elements. This enables the model behavior to be easily controllable and the desired transverse stress response in plane strain to be obtained. A two-Eyring process model has been developed on this basis to produce realistic predictions of the plane strain compression behavior of UHMWPE. Network models other than Ogden's could, in principal, be matched with flow rules that ensure the satisfaction of the condition (16).

In conventional theories, an isotropic flow rule is used that is entirely independent of the network model. This work suggests that more effective models result when there is an explicit connection between the flow rule and the network. This may

reflect a connection at a physical level, as the network develops anisotropy on straining.

The authors thank Dr Neil Hubbard of Orthoplastics Ltd., Todmorden Road, Bacup, Lancs. UK for supply of the material and also Dr. Tim Gough's support in DSC measurement and analysis and Dr. S. Naz acknowledges support of an EPSRC studentship.

References

1. Sweeney, J.; Collins, T. L. D.; Coates, P. D.; Ward, I. M. Polymer 1997, 38, 5991.
2. Arruda, E. M.; Boyce, M. C. Int J Plasticity 1993, 9, 697.
3. Arruda, E. M.; Boyce, M. C.; Quintus-Bosz, H. Int J Plasticity; 1993, 9, 783.
4. Ogden, R. W. Proc R Soc London A 1972, 326, 565.
5. Ward, I. M.; Sweeney, J.; An Introduction to the Mechanical Behaviour of Solid Polymers; Wiley: New York, 2004, Chapter 8.
6. Terentjev, E. M.; Warner, M.; Verwey, G. C. J Phys II France 1996, 6, 1049.
7. Bischoff, J. E.; Arruda, E. M.; Grosh, K. Trans ASME J Appl Mech 2002, 69, 570.
8. Horgan, C. O.; Saccomandi, G. J Mech Phys Solid 2005, 53 1985.
9. Ehret, A. E.; Itskov M. J Mater Sci 2007, 42, 8853.
10. Ogden, R. W.; Saccomandi, G. Biomech Model Mechanobiol 2007, 6, 333.
11. Van Dommelen, J. A. W.; Meijer, M. E. H. Micromechanics of Particle-Modified Semicrystalline Polymers: Influence of Anisotropy Due to Transcrystallinity and/or Flow. In: Michler GH, Baltá FJ, Eds. Mechanical Properties of Polymers Based on Nanostructure and Morphology. Taylor and Francis: Boca Raton, 2005. pp 317–378.
12. Kurtz, S. M.; Muratoglu, O. K.; Evans, M.; Edidin, A. A. Biomaterials 1999, 20, 1659.
13. Kurtz, S. M.; Villaraga, M. L.; Herr, M. P.; Bergström, J. S.; Rimnac, C. M.; Edidin, A. A. Biomaterials 2002, 23, 3681.
14. Brooks, N. W. J.; Duckett, R. A.; Ward, I. M. Polymer 1992, 33, 1872.
15. Feijoo, J. L.; Sánchez, J. J.; Műller, A. J. Polym Bull 1997, 39, 125.
16. Brooks, N. W.; J; Mukhtar, M. Polymer 2000, 41, 1475.
17. Bonet, J; Wood, R. W. Nonlinear Continuum Mechanics for Finite Element Analysis [Appendix A]. Cambridge University Press: Cambridge, 1997.
18. Buckley, C. P.; Jones, D. C. Polymer 1995, 36, 3301.
19. Spathis, G.; Kontou, E. Polym Eng Sci 2001, 41, 1337.
20. Hill, R. The Mathematical Theory of Plasticity. Oxford University Press: Oxford, 1985, Chapter 12.
21. Tzika, P. A.; Boyce, M. C.; Parks, D. M. J Mech Phys Solids 2000, 48, 1893.
22. Arruda, E. M.; Boyce, M. C. J Mech Phys Solids 1993, 41, 389.
23. Sweeney, J.; Spares, R.; Caton-Rose, P.; Coates, P.D.; J Appl Polym Sci 2007, 106, 1095.
24. Nazarenko, S.; Bensason, S.; Hiltner, A; Baer, E. Polymer 1994, 35, 3883.
25. Bauwens-Crowet, C.; Bauwens, J.-C. J Mater Sci 1972, 7, 176.
26. Govaert, L. E.; Timmermans, P. H. M.; Brekelmans, W. A. M. J Eng Mater Technol 2000, 122, 177.